The *Rad50^S* allele promotes ATM-dependent DNA damage responses and suppresses ATM deficiency: implications for the Mre11 complex as a DNA damage sensor

Monica Morales,[1,4] Jan-Willem F. Theunissen,[1,4] Carla F. Bender Kim,[2] Risa Kitagawa,[3] Michael B. Kastan,[3] and John H.J. Petrini[1,5]

[1]Molecular Biology Program, Memorial Sloan Kettering Cancer Center and Cornell University Graduate School of Medical Sciences, New York, New York 10021, USA; [2]Laboratory of Genetics, University of Wisconsin Medical School, Madison, Wisconsin 53706, USA; [3]Department of Hematology-Oncology, St Jude Children's Research Hospital, Memphis, Tennessee 38105, USA

Genetic and cytologic data from *Saccharomyces cerevisiae* and mammals implicate the Mre11 complex, consisting of Mre11, Rad50, and Nbs1, as a sensor of DNA damage, and indicate that the complex influences the activity of ataxia-telangiectasia mutated (ATM) in the DNA damage response. *Rad50$^{S/S}$* mice exhibit precipitous apoptotic attrition of hematopoietic cells. We generated ATM- and Chk2-deficient *Rad50$^{S/S}$* mice and found that *Rad50$^{S/S}$* cellular attrition was strongly ATM and Chk2 dependent. The hypomorphic *Mre11^{ATLD1}* and *Nbs1$^{\Delta B}$* alleles conferred similar rescue of *Rad50$^{S/S}$*-dependent hematopoietic failure. These data indicate that the Mre11 complex activates an ATM–Chk2-dependent apoptotic pathway. We find that apoptosis and cell cycle checkpoint activation are parallel outcomes of the Mre11 complex–ATM pathway. Conversely, the *Rad50^S* mutation mitigated several phenotypic features of ATM deficiency. We propose that the *Rad50^S* allele is hypermorphic for DNA damage signaling, and that the resulting constitutive low-level activation of the DNA damage response accounts for the partial suppression of ATM deficiency in *Rad50$^{S/S}$ Atm$^{-/-}$* mice.

[*Keywords*: Checkpoints; DNA damage signaling; apoptosis]

Supplemental material is available at http://www.genesdev.org.

Received September 9, 2005; revised version accepted October 13, 2005.

The cellular response to DNA damage includes activation of DNA damage-dependent cell cycle checkpoints, DNA repair, and in some contexts, apoptosis. The Mre11 complex, consisting of the highly conserved proteins Mre11, Rad50, and Nbs1, has been implicated in DNA damage recognition and the subsequent activation of cell cycle checkpoints, as well as in DNA repair. Human and mouse hypomorphic *Nbs1* and *Mre11* mutations (Carney et al. 1998; Stewart et al. 1999; Kang et al. 2002; Williams et al. 2002; Theunissen et al. 2003; Difilippantonio et al. 2005) in Nijmegen breakage syndrome (NBS) and the ataxia-telangiectasia-like disorder (A-TLD), respectively, are associated with ionizing radiation (IR) sensitivity, checkpoint deficiency, and chromosome instability. Despite these defects in the DNA damage response pathway, IR-dependent apoptotic induction does not appear to be compromised in *Nbs1* or *Mre11* mutant mice (Theunissen et al. 2003).

Several lines of evidence demonstrate that the Mre11 complex functions with the ataxia-telangiectasia mutated (ATM) kinase to affect aspects of the response to DNA double-strand breaks (DSBs). This conclusion is supported by molecular observations in addition to the phenotypic similarities between NBS, A-TLD, and ataxia-telangiectasia (A-T) (Petrini 2000). Nbs1 is phosphorylated by ATM in response to DNA damage, and this event is required for activation of the intra-S-phase checkpoint (Gatei et al. 2000; Lim et al. 2000; Wu et al. 2000; Zhao et al. 2000). The complex also functions upstream of ATM and possibly the ataxia-telangiectasia and Rad3-related (ATR) transducing kinase by recognizing DNA damage and potentiating their activation and activity. The complex associates with DNA damage in-

[4]These authors contributed equally to this work.
[5]Corresponding author.
E-MAIL petrinij@mskcc.org; FAX (646) 422-2062.
Article and publication are at http://www.genesdev.org/cgi/doi/10.1101/gad.1373705.

dependently of ATM or ATR, or any modifications that depend on those kinases (Petrini and Stracker 2003), and appears to recruit ATM to break sites via a conserved domain at the Nbs1 C terminus (Kitagawa et al. 2004; Falck et al. 2005; You et al. 2005). This behavior is markedly diminished in cells established from A-TLD patients (Stewart et al. 1999), and IR-dependent ATM activation is impaired as a result (Uziel et al. 2003). A similar impairment is seen in cells from NBS patients (Mochan et al. 2003; Horejsi et al. 2004). The degradation of the Mre11 complex in adenovirus-infected cells attenuates ATM activation (Stracker et al. 2002; Carson et al. 2003). Finally, Mre11 complex-dependent ATM activation has been demonstrated in vitro with purified components and in *Xenopus* extracts (Costanzo et al. 2004; Lee and Paull 2005). DNA-PKcs and SMG1(ATX) also appear to be activated by DNA damage, although the significance of the Mre11 complex in these events has not been addressed (Abraham 2004; Brumbaugh et al. 2004).

In contrast to *Nbs1* and *Mre11* mutations, the murine $Rad50^S$ allele is not associated with checkpoint deficiency, nor does it impair DSB recognition by the Mre11 complex (Bender et al. 2002). Cells from $Rad50^{S/S}$ mice exhibit indices of chronic genotoxic stress, the in vivo consequence of which is the rapid apoptotic attrition of hematopoietic and spermatogenic cells. Accordingly, p53 deficiency rescues the $Rad50^{S/S}$ phenotype. Bone-marrow depletion in $Rad50^{S/S}$ mice is primarily attributable to stem-cell failure, since $Rad50^{S/S}$ stem cells are unable to reconstitute the hematopoietic compartment in lethally irradiated wild-type mice. Because genotoxic stress in $Rad50^{S/S}$ mice is not associated with an overt DSB repair defect, and the impact of the $Rad50^S$ allele on chromosome stability is extremely mild (Bender et al. 2002; de Jager and Kanaar 2002), we have proposed that the murine $Rad50^S$ allele is an "up mutant" for activation of the DNA damage response (Stracker et al. 2004). This proposal was initially based on the hypermorphic DNA damage signaling behavior of the *Saccharomyces cerevisiae rad50S* mutant (Usui et al. 2001) and is supported by data presented herein.

In this study, we exploit the $Rad50^S$ allele to examine the Mre11 complex's role in ATM-dependent apoptosis. We show that $Rad50^{S/S}$ apoptotic attrition is mitigated in genetic contexts that impair ATM activation. Crosses between $Rad50^{S/S}$ and mutants in the ATM targets Chk2 and SMC1 revealed a branch point in the ATM-dependent apoptotic pathway. Hematopoietic attrition was rescued in $Rad50^{S/S}$ $Chk2^{-/-}$ double mutants, whereas crosses with mice expressing a *Smc1* mutant in which the two ATM phosphorylation sites Ser957 and Ser966 have been mutated had no effect (Kitagawa et al. 2004).

In ATM-deficient mice, the hypermorphic behavior of $Rad50^S$ resulted in the suppression of $Atm^{-/-}$-associated lymphomagenesis, senescence, and IR sensitivity. This suppression appeared to depend on the activation of other PI3K-like kinase family members as indicated by an increase in phoshorylated SQ/TQ motifs and γ-H2AX in $Rad50^{S/S}$ $Atm^{-/-}$. Collectively, these data demonstrate that the Mre11 complex promotes apoptotic induction in an ATM–Chk2–p53-dependent manner, and that activation of an alternative DNA damage-transducing kinase can mitigate the pathologic outcomes associated with ATM deficiency.

Results

Genetic determinants of $Rad50^{S/S}$ *pathology*

In order to determine the mechanism of $Rad50^S$-dependent cellular attrition, we defined the genetic dependencies of this $Rad50^{S/S}$ phenotypic outcome. First, to determine whether $Rad50^S$ is a hypermorphic allele, we crossed $Rad50^{S/S}$ with $Rad50^{+/\Delta}$ mice, reasoning that reduced $Rad50^S$ dosage would increase phenotypic severity if it were hypomorphic, or decrease severity if it were hypermorphic (Luo et al. 1999). Although most $Rad50^{\Delta/S}$ mice died from hematopoietic failure, the mean survival was significantly higher than that of $Rad50^{S/S}$: 58% of $Rad50^{\Delta/S}$ mice survived to 5 mo (Fig. 1A). The increased survival of $Rad50^{\Delta/S}$ was associated with malignancy as three out of 29 mice died with lymphoma (Fig. 1A). Hence, reduced $Rad50^S$ dosage in $Rad50^{\Delta/S}$ mice enhanced survival, indicating that $Rad50^S$ is a hypermorphic allele.

Since the Mre11 complex and ATM function in the same DNA damage response pathway (D'Amours and Jackson 2002; Petrini and Stracker 2003), we established $Rad50^{S/S}$ $Atm^{-/-}$ double-mutant mice to determine whether the hypermorphic character of the $Rad50^S$ allele was ATM dependent. Whereas $Rad50^{S/S}$ mice are recovered at 50% of the expected Mendelian frequency (Bender et al. 2002), $Rad50^{S/S}$ $Atm^{-/-}$ mice were recovered at normal Mendelian ratios.

Phenotypic rescue was also observed in mature animals. Peripheral blood cell numbers in $Rad50^{S/S}$ $Atm^{-/-}$ mice were comparable to wild-type levels (red blood cell percentages: wild type, 41%; $Rad50^{S/S}$, 32%; $Rad50^{S/S}$ $Atm^{-/-}$, 39%; platelet numbers: wild type, 575×10^3 cells/mL; $Rad50^{S/S}$, 252×10^3 cells/mL; $Rad50^{S/S}$ $Atm^{-/-}$, 500×10^3 cells/mL). Flow cytometry on 4-wk-old mice indicated that hematopoietic cells in both $Rad50^{S/S}$ $Atm^{+/-}$ and $Rad50^{S/S}$ $Atm^{-/-}$ mice were comparable to those in $Atm^{-/-}$ mice (Fig. 2; Supplementary Table 1). The rescue of $Rad50^{S/S}$ hematopoietic attrition was associated with significantly increased survival of $Rad50^{S/S}$ $Atm^{+/-}$ and $Rad50^{S/S}$ $Atm^{-/-}$ mice compared with $Rad50^{S/S}$ (Fig. 1B). Whereas most (>90%) $Rad50^{S/S}$ mice died during the first 5 mo of age, 85% of $Rad50^{S/S}$ $Atm^{+/-}$ mice and 42% of $Rad50^{S/S}$ $Atm^{-/-}$ mice lived longer than 5 mo. The increase in survival relative to $Rad50^{S/S}$ alone was significant at 5, 10, and 15 mo of age (P values < 0.001). $Rad50^{S/S}$ $Atm^{-/-}$ died of malignancy and $Rad50^{S/S}$ $Atm^{+/-}$ predominantly succumbed to anemia, albeit significantly later than most $Rad50^{S/S}$ mice. The data indicated that the attrition of hematopoietic cells in $Rad50^{S/S}$ mice was dependent on ATM.

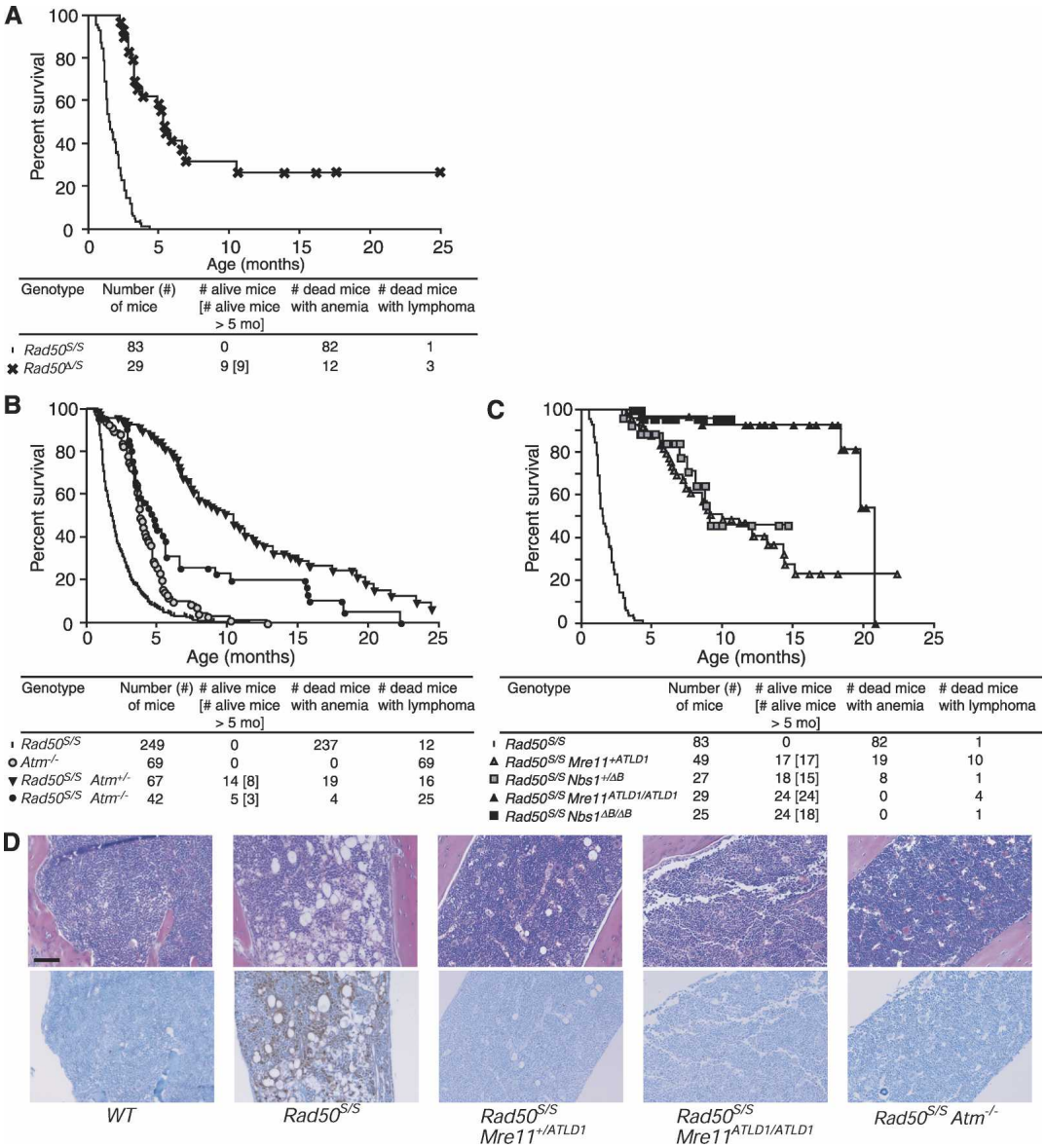

Genotype	Number (#) of mice	# alive mice [# alive mice > 5 mo]	# dead mice with anemia	# dead mice with lymphoma
$Rad50^{S/S}$	83	0	82	1
$Rad50^{\Delta/S}$	29	9 [9]	12	3

Genotype	Number (#) of mice	# alive mice [# alive mice > 5 mo]	# dead mice with anemia	# dead mice with lymphoma
$Rad50^{S/S}$	249	0	237	12
$Atm^{-/-}$	69	0	0	69
$Rad50^{S/S}$ $Atm^{+/-}$	67	14 [8]	19	16
$Rad50^{S/S}$ $Atm^{-/-}$	42	5 [3]	4	25

Genotype	Number (#) of mice	# alive mice [# alive mice > 5 mo]	# dead mice with anemia	# dead mice with lymphoma
$Rad50^{S/S}$	83	0	82	1
$Rad50^{S/S}$ $Mre11^{+ATLD1}$	49	17 [17]	19	10
$Rad50^{S/S}$ $Nbs1^{+/\Delta B}$	27	18 [15]	8	1
$Rad50^{S/S}$ $Mre11^{ATLD1/ATLD1}$	29	24 [24]	0	4
$Rad50^{S/S}$ $Nbs1^{\Delta B/\Delta B}$	25	24 [18]	0	1

Figure 1. Rescue of $Rad50^{S/S}$ survival by *Rad50*-null, *Atm*-null, $Mre11^{ATLD1}$, and $Nbs1^{\Delta B}$ alleles. (*A*) Kaplan-Meier survival curves of $Rad50^{S/S}$ and $Rad50^{\Delta/S}$ mice. (*B*) Kaplan-Meier survival curves of $Rad50^{S/S}$, $Atm^{-/-}$, $Rad50^{S/S}$ $Atm^{+/-}$, and $Rad50^{S/S}$ $Atm^{-/-}$ mice. (*C*) Kaplan-Meier survival curves of $Rad50^{S/S}$, $Rad50^{S/S}$ $Mre11^{+/ATLD1}$, $Rad50^{S/S}$ $Mre11^{ATLD/ATLD1}$, $Rad50^{S/S}$ $Nbs1^{+/\Delta B}$, and $Rad50^{S/S}$ $Nbs1^{\Delta B/\Delta B}$ mice. (*A–C*) In each table *below* the survival curves, for each cohort, the number of mice that were found dead without overt signs of anemia and malignancy is equal to the number of mice minus the number of alive mice, the number of dead mice with anemia, and the number of dead mice with lymphoma. (*D*) Hematoxylin and eosin staining (*upper* pictures) or cleaved Caspase-3 detected by immunohistochemistry (*lower* pictures) in bone marrow sections from 4-wk-old $Rad50^{S/S}$, $Rad50^{S/S}$ $Atm^{-/-}$, $Rad50^{S/S}$ $Mre11^{+/ATLD1}$, and $Rad50^{S/S}$ $Mre11^{ATLD/ATLD1}$ mice. Magnification, 100×. Bar, 100 μM.

Genetic interactions with Mre11 complex mutants

As with cells established from A-TLD patients, cells from mice expressing the $Mre11^{ATLD1}$ allele ($Mre11^{ATLD1/ATLD1}$ mice) exhibit indices of attenuated ATM activity (Theunissen et al. 2003). We established $Rad50^{S/S}$ $Mre11^{ATLD1/ATLD1}$ double mutants to determine whether reduced ATM activation by the Mre11 complex would also rescue $Rad50^{S/S}$ cellular attrition. As with the *Atm*-null allele, $Mre11^{ATLD1}$ increased $Rad50^{S/S}$ survival in a dose-dependent manner (Fig. 1C). Cohorts of 29 $Rad50^{S/S}$ $Mre11^{ATLD1/ATLD1}$ and 49 $Rad50^{S/S}$ $Mre11^{+/ATLD1}$ mice were aged and monitored for indications of $Rad50^{S/S}$-dependent pathology. Twenty-four out of 29 $Rad50^{S/S}$ $Mre11^{ATLD1/ATLD1}$ mice were alive and older than 5 mo with no overt signs of anemia at the time of this writing, and four double mutants developed lymphoma.

A similar, but less pronounced rescue was observed in $Rad50^{S/S}$ $Mre11^{+/ATLD1}$ mice. Seventeen $Rad50^{S/S}$

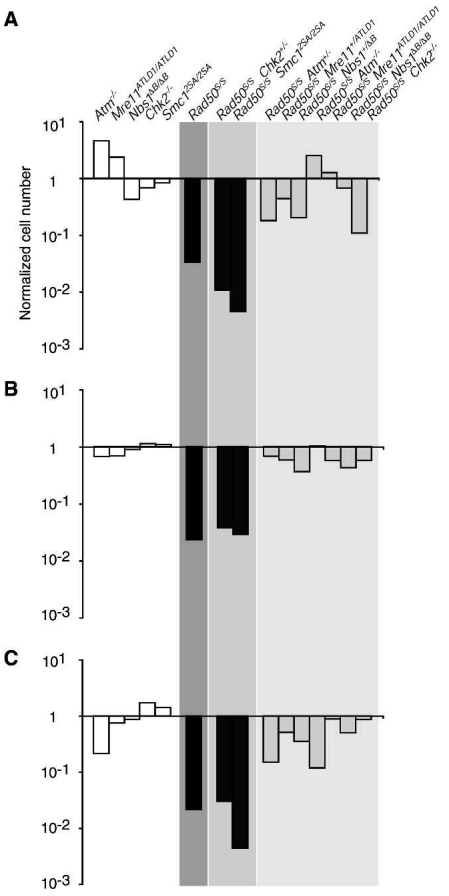

Figure 2. Rescue of $Rad50^{S/S}$ hematopoietic attrition by *Atm*-null, $Mre11^{ATLD1}$, and $Nbs1^{\Delta B}$ alleles, and by $Chk2^{-/-}$. Flow cytometric analysis of hematopoietic tissues from 4–9-wk-old mice. The numbers of double-negative T cells in the thymus (DN T cells; *A*), and macrophages (*B*) and pro-B cells in the bone marrow (*C*), normalized to wild-type data, are depicted for the indicated genotypes.

$Mre11^{+/ATLD1}$ mice were alive and older than 5 mo. Out of the 32 $Rad50^{S/S}$ $Mre11^{+/ATLD1}$ mice that died, 19 exhibited hematopoietic attrition, 10 succumbed to lymphoma, and three died without signs of anemia and malignancy (Fig. 1C). Flow-cytometric analysis of bone marrow from 6-wk-old animals confirmed that increased survival in $Rad50^{S/S}$ $Mre11^{ATLD1/ATLD1}$ and $Rad50^{S/S}$ $Mre11^{+/ATLD1}$ was associated with reduced hematopoietic attrition. The numbers of double-negative (DN) T cells, pro-B cells, and macrophages in both $Rad50^{S/S}$ $Mre11^{ATLD1/ATLD1}$ and $Rad50^{S/S}$ $Mre11^{+/ATLD1}$ were within 2.5-fold of wild-type levels, showing that $Rad50^{S/S}$ hematopoietic attrition was affected by a single copy of $Mre11^{ATLD1}$ (Fig. 2; Supplementary Table 1).

$Nbs1^{\Delta B/\Delta B}$ mice also exhibit reduced indices of ATM activity (Williams et al. 2002). Similar to the hematopoietic rescue of $Rad50^{S/S}$ by $Mre11^{ATLD1}$, the numbers of DN T cells, pro-B cells, and macrophages in both $Rad50^{S/S}$ $Nbs1^{\Delta B/\Delta B}$ and $Rad50^{S/S}$ $Nbs1^{+/\Delta B}$ were within fivefold of wild-type levels (Fig. 2; Supplementary Table 1). As with *ATM* and *MRE11*, the increase in $Rad50^{S/S}$ survival was dependent on *NBS1* gene dosage (Fig. 1C).

Rad50$^{S/S}$ *cellular attrition is due to apoptosis*

Attrition of $Rad50^{S/S}$ hematopoietic cells was attributable to apoptosis. Immunohistochemical analysis of $Rad50^{S/S}$ bone marrow revealed markedly increased levels of cleaved Caspase-3, whereas wild type did not show appreciable staining (Fig. 1D). The staining of cleaved Caspase-3 was reduced to wild-type levels in $Rad50^{S/S}$ $Atm^{-/-}$, $Rad50^{S/S}$ $Mre11^{ATLD1/ATLD1}$, and $Rad50^{S/S}$ $Mre11^{+/ATLD1}$ bone marrow (Fig. 1D). Similar results were obtained in thymus and testes sections (data not shown). This interpretation was further supported by genetic evidence. We crossed $Rad50^{S/S}$ with *Eμ-Bcl2* mice, which carry a transgene of the anti-apoptotic *BCL2* gene (Strasser et al. 1990). This transgene increases resistance to apoptosis in B and T lymphocytes (Strasser et al. 1991a,b). The depletion of hematopoietic stem cells in $Rad50^{S/S}$ mice appears to be partially attributable to the attrition of committed precursors (Bender et al. 2002). Therefore, we reasoned that reduction in the loss of B and T cells in $Rad50^{S/S}$ *Eμ-Bcl2* would confer increased survival. This was indeed the case, as $Rad50^{S/S}$ *Eμ-Bcl2* mice succumbed to anemia significantly later than $Rad50^{S/S}$ (Fig. 3A). These observations confirm that apoptosis underlies the precipitous $Rad50^{S/S}$ hematopoietic failure, consistent with the previously established p53 dependency for $Rad50^{S/S}$ cellular attrition (Bender et al. 2002). Collectively, the experiments in which reduced ATM activity rescues $Rad50^{S/S}$ hematopoiesis demonstrate that $Rad50^{S/S}$, and by extension, the Mre11 complex, promotes ATM-dependent apoptosis.

Genetic interactions with downstream ATM targets

To define the ATM targets that are activated in this context, we crossed $Rad50^{S/S}$ with $Chk2^{-/-}$ and $Smc1^{S957AS966A/S957AS966A}$ ($Smc1^{2SA/2SA}$) mutant mice (Hirao et al. 2002; Kitagawa et al. 2004). $Rad50^{S/S}$ $Chk2^{-/-}$ hematopoietic cell numbers were within twofold of wild type (Fig. 2; Supplementary Table 1). In our cohort of $Rad50^{S/S}$ $Chk2^{-/-}$ mice, 52 out of 65 were alive and older than 5 mo at the time of this writing (Fig. 3B). Although less pronounced than with *ATM*, *MRE11*, or *NBS1*, the rescue of $Rad50^{S/S}$ survival by Chk2 deficiency was partially dependent on gene dosage, with 10 of 41 $Rad50^{S/S}$ $Chk2^{+/-}$ mice alive at 5 mo-of-age (Fig. 3B).

In contrast, $Rad50^{S/S}$ $Smc1^{2SA/2SA}$ mice were indistinguishable from $Rad50^{S/S}$ with respect to hematopoietic cell numbers and survival (Figs. 2, 3B). These data demonstrate that $Rad50^{S/S}$ activates Mre11 complex ATM-dependent apoptosis through the Chk2 kinase. Given that phosphorylation of SMC1 by ATM is necessary for activation of the intra-S-phase checkpoint (Kim et al. 2002; Yazdi et al. 2002; Kitagawa et al. 2004), the data further indicate that apoptotic induction and intra-S-phase checkpoint activation are parallel endpoints of the Mre11 complex–ATM pathway.

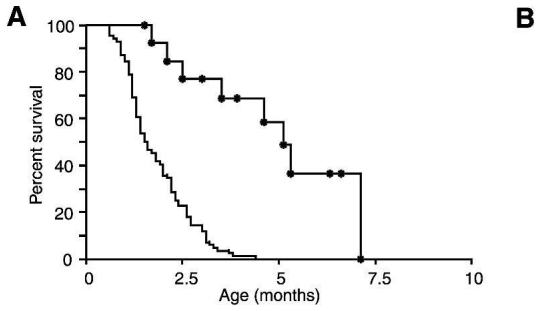

Genotype	Number (#) of mice	# alive mice [# alive mice > 5 mo]	# dead mice with anemia	# dead mice with lymphoma
▪ *Rad50*$^{S/S}$	83	0	82	1
● *Rad50*$^{S/S}$ *Eμ-Bcl2*	15	7 [3]	5	0

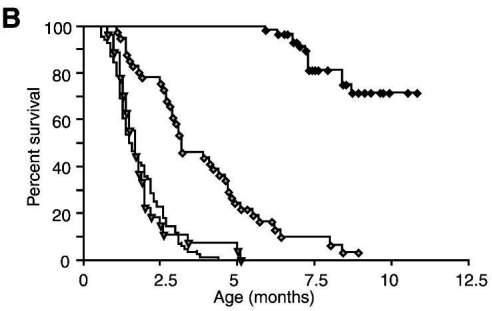

Genotype	Number (#) of mice	# alive mice [# alive mice > 5 mo]	# dead mice with anemia	# dead mice with lymphoma
▪ *Rad50*$^{S/S}$	83	0	82	1
◇ *Rad50*$^{S/S}$ *Chk2*$^{+/-}$	41	3 [3]	36	2
▽ *Rad50*$^{S/S}$ *Smc1*$^{2SA/2SA}$	27	0 [0]	26	1
◆ *Rad50*$^{S/S}$ *Chk2*$^{-/-}$	65	52 [52]	0	10

Figure 3. Rescue of *Rad50*$^{S/S}$ survival by *Chk2*-null allele and the *Eμ-Bcl2* transgene. (*A*) Kaplan-Meier survival curves of *Rad50*$^{S/S}$ and *Rad50*$^{S/S}$ *Eμ-Bcl2* mice. (*B*) Kaplan-Meier survival curves of *Rad50*$^{S/S}$, *Rad50*$^{S/S}$ *Chk2*$^{+/-}$, *Rad50*$^{S/S}$ *Chk2*$^{-/-}$, and *Rad50*$^{S/S}$ *Smc1*$^{2SA/2SA}$ mice. Each table *below* the survival curves is as in Figure 1.

ATM-dependent signaling was examined at the molecular level to identify the targets responsible for the *Rad50*$^{S/S}$ apoptotic phenotype. Irradiation induces autophosphorylation of ATM Ser1981, and this phosphorylation event correlates with ATM activation (Bakkenist and Kastan 2003). In asynchronous primary ear fibroblast cultures, phosphorylation of ATM Ser1981 was increased in unirradiated *Rad50*$^{S/S}$ cells compared with wild type (Fig. 4A). This outcome was associated with phosphorylation in untreated cells of the ATM targets H2AX (Fig. 5D), 53BP1 (Fig. 4B), and SMC1 (Fig. 4C) on Ser139, Ser25, and Ser957, respectively. Constitutive ATM autophosphorylation (Fig. 4A) and SMC1 phosphorylation were reduced in the genetic contexts that led to enhanced *Rad50*$^{S/S}$ survival, (i.e., *Rad50*$^{S/S}$ *Mre11*$^{ATLD1/ATLD1}$, *Rad50*$^{S/S}$ *Atm*$^{+/-}$, and moderate reduction in *Rad50*$^{S/S}$ *Mre11*$^{+/ATLD1}$) (Fig. 4C), consistent with the interpretation that ATM-dependent signaling accounts for cellular attrition in *Rad50*$^{S/S}$.

Rad50$^{S/S}$ *suppresses ATM deficiency*

Remarkably, the phenotypic rescue in *Rad50*$^{S/S}$ *Atm*$^{-/-}$ was bidirectional. Whereas the data clearly demonstrated that the Mre11 complex activates ATM-dependent apoptotic pathways, *Rad50*$^{S/S}$ *Atm*$^{-/-}$ exhibited an additional striking feature. The latency of lymphomagenesis associated with ATM deficiency was profoundly increased in *Rad50*$^{S/S}$ *Atm*$^{-/-}$ double mutants. The majority of *Atm*$^{-/-}$ mice in our colony died with thymic lymphomas by 5 mo of age, 2.9% lived to 10 mo, and none lived beyond 15 mo (Fig. 1B). In contrast, *Rad50*$^{S/S}$ *Atm*$^{-/-}$ mice showed increased survival compared with *Atm*$^{-/-}$ mice: 20.5% of *Rad50*$^{S/S}$ *Atm*$^{-/-}$ mice survived to 10 mo ($P < 0.005$) and 18% survived to 15 mo ($P < 0.001$). It is conceivable that the increased latency of lymphomagenesis is due to a qualitative difference between the lymphomas arising in *Atm*$^{-/-}$ versus *Rad50*$^{S/S}$ *Atm*$^{-/-}$ mice. Unlike *Atm*$^{-/-}$ mice, T-cell development in *Rad50*$^{S/S}$ *Atm*$^{-/-}$ mice was essentially the same as in wild-type mice (data not shown).

To analyze the mechanism(s) by which the *Rad50*^{S} allele suppressed ATM deficiency, we assessed DNA damage signaling in primary *Rad50*$^{S/S}$ *Atm*$^{-/-}$ cells. Substrates of the three ATM-related kinases, ATM, DNA-PKcs, and ATR have SQ/TQ motifs at the site of phosphorylation (Kim et al. 1999). We reasoned that a general assessment of DNA damage signaling in *Rad50*$^{S/S}$ and *Rad50*$^{S/S}$ *Atm*$^{-/-}$ cells could be obtained by immunofluorescence experiments using phospho-SQ/TQ antiserum. This approach has recently been applied to the analysis of Mlh1-dependent checkpoint signaling (Stojic et al. 2004). Consistent with the previous data indicating constitutive DNA damage signaling, SQ/TQ foci were observed in unirradiated *Rad50*$^{S/S}$ cells at a significantly higher frequency than in wild-type cells (Fig. 5A,B). After γ-irradiation, >90% of wild-type and *Rad50*$^{S/S}$ cells formed foci, whereas only 16% of *Atm*$^{-/-}$ fibroblasts had foci. *Rad50*$^{S/S}$ *Atm*$^{-/-}$ fibroblasts exhibited SQ/TQ foci in 36% of the cells (Fig. 5A). Focus formation was reduced in caffeine (20 mM)-treated *Rad50*$^{S/S}$ *Atm*$^{-/-}$ cells (Fig. 5C), and partial colocalization with 53BP1 foci was observed in all genotypes studied (data not shown). Although we cannot rule out the possibility that *Rad50*$^{S/S}$ cells exhibit a small amount of DNA damage, these data suggest that *Rad50*^{S} activates a compensating DNA damage response pathway that leads to the rescue of ATM deficiency.

H2AX phosphorylation to create γ-H2AX is another general indicator of DNA damage signaling. This event can be effected by ATM, ATR, or DNA-PKcs according to the experimental setting (Burma et al. 2001; Ward and Chen 2001). Consistent with previous data (Bender et al. 2002), γ-H2AX was present in untreated *Rad50*$^{S/S}$ mouse embryonic fibroblasts (MEFs) (Fig. 5D). γ-H2AX formation was observed in response to camptothecin (CPT), hydroxyurea (HU), ultraviolet light (UV), and IR treatment in wild-type and *Rad50*$^{S/S}$ MEFs. *Atm*$^{-/-}$ cells ex-

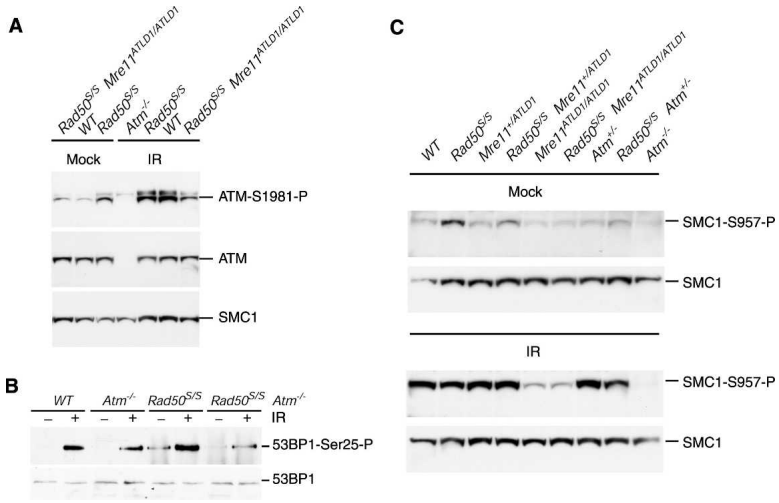

Figure 4. Constitutive ATM activity in $Rad50^{S/S}$ is rescued by ATM deficiency and $Mre11^{ATLD1}$. (*A*) Analysis of ATM Ser1981 phosphorylation. Extracts from wild-type (WT), $Rad50^{S/S}$, $Rad50^{S/S}$ $Mre11^{ATLD1/ATLD1}$, and $Atm^{-/-}$ p4 ear fibroblasts were prepared after mock treatment and 1 h after 10 Gy of IR. For the ATM Ser1981 phosphorylation Western blot (ATM-Ser1981-P), the lower reactive species represents ATM, as indicated by the ATM Western blot (ATM), and the upper band is nonspecific. SMC1 is included as a loading control. (*B*) Analysis of 53BP1 phosphorylation in primary ear fibroblasts. Ser25-phosphorylated 53BP1 was immunoprecipitated from untreated or irradiated (10 min after 4 Gy) primary ear fibroblast extracts, and detected with a 53BP1 antibody. A 53BP1 Western blot of the same extracts is shown as a loading control. (*C*) Analysis of SMC1 Ser 957 phosphorylation in the indicated mutants. Extracts from p4 ear fibroblasts were prepared after mock treatment and 1 h after 10 Gy of IR. The extracts were sequentially immunoblotted with SMC1-Ser957-P and SMC1 (loading control) antisera. (WT) Mock-treated wild-type lane underloaded for SMC1. As untreated $Mre11^{+/ATLD1}$ cells were equivalent to wild type for the levels of SMC1 phosphorylation (data not shown), compare mutants with that lane.

hibited weak γ-H2AX signal following camptothecin, HU, and UV, whereas signal was absent following IR. In contrast, substantial γ-H2AX formation was seen in $Rad50^{S/S}$ $Atm^{-/-}$ cells following all treatments, including IR (Fig. 5D).

These molecular indices were associated with the mitigation of cellular phenotypic features in $Rad50^{S/S}$ $Atm^{-/-}$ cells. Cultured $Atm^{-/-}$ MEFs exhibit senescence-like proliferative failure (Barlow et al. 1996; Xu and Baltimore 1996). In contrast, the growth of $Rad50^{S/S}$ $Atm^{-/-}$ MEFs was comparable to wild type and $Rad50^{S/S}$ (Fig. 6A). $Rad50^{S/S}$ $Atm^{-/-}$ cells were also significantly more radioresistant than $Atm^{-/-}$ cells, with the double mutants approximating wild-type and $Rad50^{S/S}$ survival at low IR doses (Fig. 6B). The enhanced radioresistance, as well as the increase in SQ/TQ foci formation, is not an effect of cell cycle distribution (data not shown). $Rad50^{S/S}$ did not reduce $Mre11^{ATLD1/ATLD1}$ IR sensitivity, as both $Mre11^{ATLD1/ATLD1}$ and $Rad50^{S/S}$ $Mre11^{ATLD1/ATLD1}$ MEFs exhibited the same degree of IR sensitivity (Fig. 6C).

In addition, $Rad50^{S/S}$ $Atm^{-/-}$ cells had a slight reduction in chromosome instability relative to $Atm^{-/-}$; however, $Rad50^{S/S}$ had no effect on instability in $Mre11^{ATLD1/ATLD1}$ (Supplementary Tables 2, 3).

Although certain aspects of ATM deficiency were substantially mitigated in $Rad50^{S/S}$ $Atm^{-/-}$ mice, the effect was relatively circumscribed. $Rad50^{S/S}$ did not rescue the IR-induced G1/S, intra-S-phase, and G2/M checkpoint defects in $Atm^{-/-}$ or $Mre11^{ATLD1/ATLD1}$ (Supplementary Fig. 1A–C). Nor did $Rad50^{S/S}$ rescue the IR-dependent $Atm^{-/-}$ phosphorylation defects on 53BP1 Ser25 (Fig. 4B), SMC1 Ser957, Chk2, and p53 Ser18 (Fig. 4C; Supplementary Fig. 1D), or the IR-dependent $Mre11^{ATLD1/ATLD1}$ and $Nbs1^{\Delta B/\Delta B}$ phosphorylation defects on SMC1 Ser957 and Chk2 (Supplementary Fig. 1D). This suggests that the alternative pathway activated by $Rad50^{S}$ has a relatively limited overlap with the canonical ATM pathway.

Discussion

In this study, we exploit the behavior of the $Rad50^{S}$ allele to examine the Mre11 complex's role in promoting apoptosis. We show that the precipitous apoptotic attrition of hematopoietic cells in $Rad50^{S/S}$ mice is abrogated by ATM deficiency. Consistent with the ATM dependence of this rescue, hypomorphic mutations in the Mre11 complex ($Mre11^{ATLD1}$ and $Nbs1^{\Delta B}$ alleles) that are associated with reduced ATM activity also abrogate $Rad50^{S/S}$ cellular attrition. Similar rescue is effected by Chk2 and p53 deficiency. These data indicate that the Mre11 complex governs an ATM–Chk2–p53-dependent apoptotic pathway. Our results further indicate that in addition to the aforementioned ATM-dependent apoptotic pathway, $Rad50^{S}$ also partially suppresses the lymphomagenesis, senescence, and radiosensitivity associated with ATM deficiency by activating a compensating pathway.

Parallel endpoints of the Mre11 complex–ATM DNA damage response pathway

Whereas it is well-established that the Mre11 complex and ATM collaborate in the activation of cell cycle checkpoints, (D'Amours and Jackson 2002; Stracker et al. 2004), these data provide the first indication that the Mre11 complex has an effect on ATM-dependent apoptosis. This finding was somewhat unexpected as neither $Nbs1^{\Delta B/\Delta B}$ nor $Mre11^{ATLD1/ATLD1}$ mice exhibit defects in IR-induced thymocyte apoptosis (Theunissen et al. 2003). Hematopoietic attrition in $Rad50^{S/S}$ mice is rescued by reduced ATM dosage, and by two Mre11 complex mutations that attenuate ATM activity, the $Mre11^{ATLD1}$ allele (Theunissen et al. 2003) and the

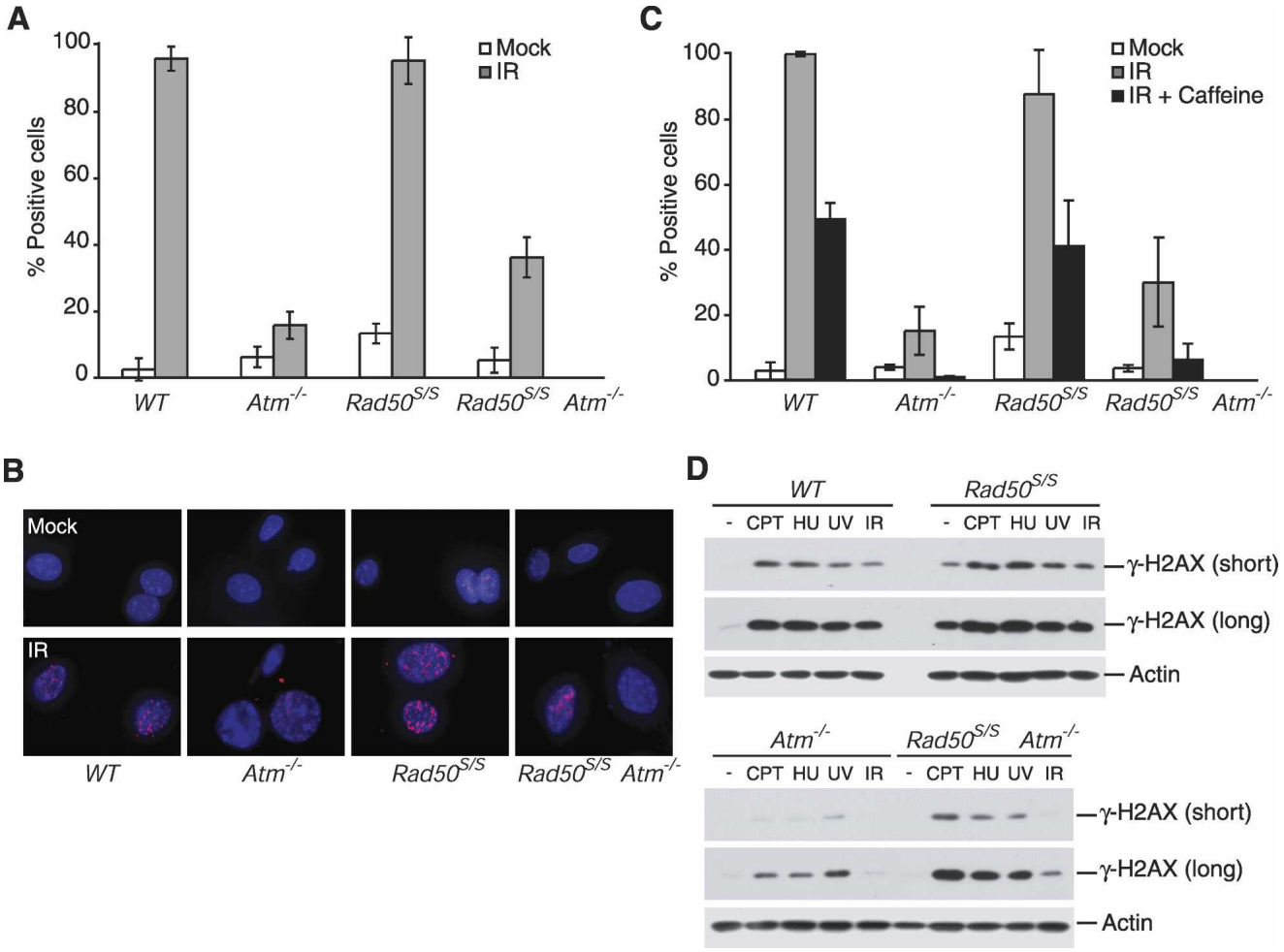

Figure 5. DNA damage signaling is enhanced in $Rad50^{S/S}$ $Atm^{-/-}$ cells compared with $Atm^{-/-}$ cells. (*A*) SQ/TQ foci formation in wild-type (WT), $Atm^{-/-}$, $Rad50^{S/S}$, and $Rad50^{S/S}$ $Atm^{-/-}$ primary ear fibroblasts was assessed by immunofluorescence. Primary ear fibroblasts were harvested 30 min after mock treatment (white bars) or 4 Gy of IR (gray bars). Two-hundred-fifty cells were counted for presence or absence of SQ/TQ foci. A cell is considered positive when it shows ≥10 foci. Data are from three experiments. (*B*) SQ/TQ foci from mock-treated or 4 Gy-irradiated primary ear fibroblasts. (*C*) Primary ear fibroblasts were pretreated for 1 h with caffeine (20 mM) or vehicle and harvested 30 min after treatment with 4 Gy IR as indicated. For each treatment, 250 cells were counted for presence or absence of SQ/TQ foci. Data are from two experiments run in duplicate. (*D*) Extracts from primary MEF cultures prepared after mock treatment (–); 1 h after 1 μM CPT, 2 mM HU, or 20 J/m^2 UV; or 10 min after 5 Gy of IR treatment were sequentially immunoblotted with γ-H2AX and Actin (loading control) antisera. "Short" and "Long" represent short and long exposure, respectively.

$Nbs1^{\Delta B}$ allele (Williams et al. 2002). Accordingly, levels of cleaved Caspase-3 are reduced in the thymus and bone marrow of these mice. $Rad50^{S/S}$ *Eμ-bcl-2* mice also exhibit significantly increased survival compared with $Rad50^{S/S}$, confirming that the $Rad50^{S}$ allele activates apoptosis. Chk2 and p53 are the downstream regulators of the apoptotic pathway governed by the Mre11 complex, since deficiency of those proteins abrogates the rapid apoptotic attrition seen in $Rad50^{S/S}$ mice (Bender et al. 2002; this study).

The Mre11 complex's influence on apoptosis was separable from its influence on checkpoint activation. SMC1 is phosphorylated by ATM following DNA damage. This event is dependent upon the Mre11 complex and is required for activation of the intra-S-phase checkpoint (Kim et al. 2002; Yazdi et al. 2002; Kitagawa et al. 2004). SMC1 is constitutively phosphorylated in $Rad50^{S/S}$ mice. This outcome is abrogated by ATM deficiency and $Mre11^{ATLD1}$. We reasoned that if apoptosis were a downstream consequence of SMC1 phosphorylation, $Smc1^{2SA/2SA}$ would rescue $Rad50^{S/S}$ cellular attrition. However, $Smc1^{2SA/2SA}$ had no effect on the $Rad50^{S/S}$ phenotype, indicating that SMC1 is not in the apoptotic pathway governed by the Mre11 complex. Thus, SMC1 defines a branch in the Mre11 complex–ATM pathway, and apoptosis and checkpoint activation are parallel outcomes of the pathway. Collectively, these data reveal that the Mre11 complex is required for ATM to initiate parallel DNA damage responses, leading to the regulation of chromosome stability and cell cycle checkpoints on one hand, and to the induction of apoptosis on the other.

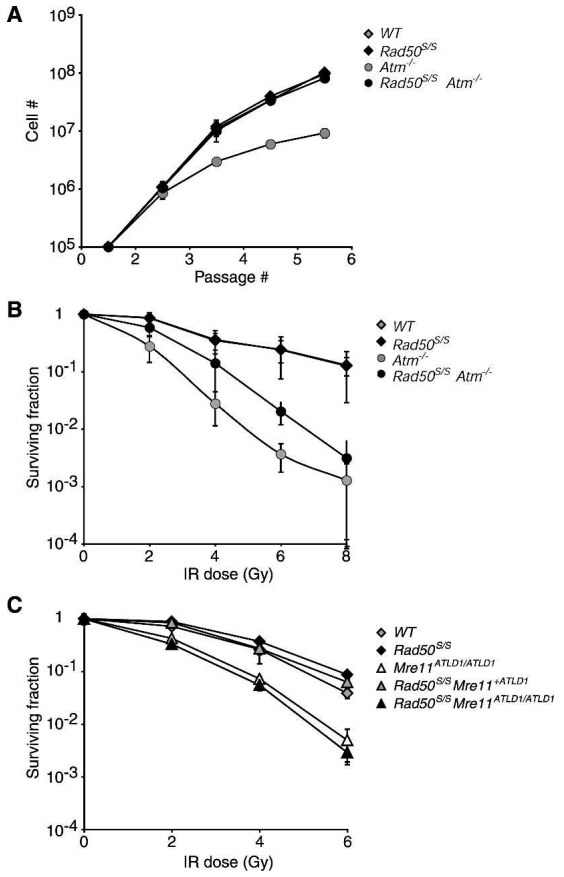

Figure 6. *Rad50^S* rescues the growth defects and IR-sensitivity of *Atm*$^{-/-}$ cells. (*A*) Cumulative growth curve. Passage 2 MEFs from two cultures were seeded in triplicate onto 6-well plates, counted every 3 d, and replated for four passages. Genotypes as indicated. (*B*,*C*) IR sensitivity determined by colony forming assay. (*B*) The surviving fractions of wild-type (WT), *Atm*$^{-/-}$, *Rad50$^{S/S}$*, and *Rad50$^{S/S}$ Atm*$^{-/-}$ SV40-transformed MEFs after various doses of IR are shown. Note that the wild-type and *Rad50$^{S/S}$* curves overlap. Graph contains data from three independent experiments in which cells were plated in triplicate at each dose. Similar results were obtained with SV40-transformed ear fibroblasts. (*C*) The surviving fractions of wild-type (WT), *Mre11$^{ATLD/ATLD1}$*, *Rad50$^{S/S}$*, *Rad50$^{S/S}$ Mre11$^{+/ATLD1}$*, and *Rad50$^{S/S}$ Mre11$^{ATLD/ATLD1}$* SV40-transformed MEFs after various doses of IR are shown.

Possible mechanisms of Rad50^S*-dependent pathology*

The molecular basis of chronic DNA damage signaling in *Rad50$^{S/S}$* is not clear. We have proposed that in *S. cerevisiae* and mammals, the Rad50S-containing Mre11 complex is an up-mutant for DNA damage signaling, and in this regard, may analogize a receptor mutant in which a signaling takes place in the absence of ligand—in this speculative scenario, the ligand in question would be DNA damage (Petrini and Stracker 2003). This hypothesis is based in part on the observation that, despite indices of chronic genotoxic stress, no evidence for the accumulation of DNA damage in either *S. cerevisiae* or murine *Rad50^S* mutants has been obtained, and neither organism exhibits overt DNA repair defects.

Several lines of evidence from this study support this hypothesis. Reducing *Rad50^S* dosage (in *Rad50$^{\Delta/S}$* mice) enhances survival. If *Rad50^S* were a hypomorphic allele that affected Mre11 complex-mediated DNA repair, *Rad50$^{\Delta/S}$* would likely exhibit a more severe phenotype than *Rad50$^{S/S}$*. The fact that neither *Nbs1$^{\Delta B/\Delta B}$* nor *Mre11$^{ATLD1/ATLD1}$*, both of which are bona fide hypomorphic mutants, enhance the severity of *Rad50$^{S/S}$* is also inconsistent with the idea that impaired DNA damage metabolism underlies the *Rad50$^{S/S}$* phenotype. The Mre11 complex's cytologic behavior is normal in *Rad50$^{S/S}$* cells (Bender et al. 2002), and we have not observed a significant increase in Rad51 spontaneous foci (data not shown). These observations, together with the fact that *Rad50$^{S/S}$* cells do not exhibit sensitivity to a broad range of clastogens (Bender et al. 2002), support the interpretation that the enhanced signaling in *Rad50$^{S/S}$* is not due to a defect in DSB repair. Finally, the *Rad50^S* allele's extremely mild effect on chromosome stability would appear to be insufficient to account for the severity of its effect on apoptosis (Bender et al. 2002; de Jager and Kanaar 2002). For comparison, nothing resembling the *Rad50$^{S/S}$* phenotype is seen in murine mutants associated with chromosome instability or DNA repair defects. Some examples include *Mre11$^{ATLD1/ATLD1}$* mice (Theunissen et al. 2003), *Ku* (Difilippantonio et al. 2000), *scid* (Bosma et al. 1983), *Rad54* (Essers et al. 1997), *Mus81* (McPherson et al. 2004), *Brca1* (Ludwig et al. 2001), and *H2AX* (Bassing et al. 2003; Celeste et al. 2003). Notably, the level of chromosome breakage, both spontaneous and induced, appears to be substantially higher in *Mre11$^{ATLD1/ATLD1}$* mice than in the strains noted above, yet bears no phenotypic resemblance to *Rad50$^{S/S}$*.

An alternative, nonexclusive hypothesis is also supported by the data. The promotion of apoptosis by the *Rad50^S* allele may reflect a gain of function that leads to the induction or stabilization of a unique lesion. This lesion would necessarily be one that is not a major product of the clastogenic agents we have used (IR, mitomycin C, or HU), as no sensitivity of *Rad50$^{S/S}$* cells to those agents is evident (Bender et al. 2002; data not shown). Supporting this possibility is the fact that *Rad50$^{S/S}$* double mutants in which cellular attrition is attenuated are frequently associated with lymphomagenesis. *Rad50$^{S/S}$ Chk2*$^{-/-}$ is particularly affected; 10 of the 12 mice died with lymphoma (Fig. 3B). It is important to consider that the lesion hypothesis does not exclude the possibility that *Rad50$^{S/S}$* is hypermorphic for signaling, and that the *Rad50$^{S/S}$* phenotype may be a composite outcome of the two.

An intriguing possibility for the *Rad50$^{S/S}$*-dependent lesion is a covalent DNA–protein complex. The Mre11 complex is implicated in the nucleolytic removal of covalently attached topoisomerase II or topoisomerase II-like proteins in bacteriophage T4 and *S. cerevisiae* (Keeney and Kleckner 1995; Nairz and Klein 1997; Tsubouchi and Ogawa 1998; Stohr and Kreuzer 2001). For example, the removal of Spo11 from meiotic DSBs is completely blocked in *S. cerevisiae rad50S* mutants (Keeney and Kleckner 1995). Recent data demonstrate that Spo11 is

removed from DSB ends by endonucleolytic cleavage adjacent to the bound protein in both *S. cerevisiae* and mice, and further, that this mode of repair may be generally relevant to the removal of covalent topoisomerase II cleavage complexes (Neale et al. 2005). The involvement of the Mre11 complex in this repair process remains to be addressed.

Activation of an alternative DNA damage response pathway in Rad50$^{S/S}$ *mice*

An equally striking aspect of *Rad50$^{S/S}$* is its effect on ATM deficiency. *Rad50$^{S/S}$* rescues the lymphomagenesis, senescence, and radiosensitivity of ATM-deficient mice and cells. This rescue is associated with enhancement of several generic readouts of ATM/ATR signaling in *Rad50$^{S/S}$ Atm$^{-/-}$* cells. For example, SQ/TQ foci form in response to IR treatment at a higher frequency in *Rad50$^{S/S}$ Atm$^{-/-}$* compared with *Atm$^{-/-}$* fibroblasts. Since this outcome is blocked by caffeine treatment, the data suggest that *Rad50$^{S/S}$* activates a PI3K-like kinase with overlapping specificity to that of ATM. In addition, γ-H2AX formation after treatment with several DNA damaging agents is enhanced in *Rad50$^{S/S}$ Atm$^{-/-}$* MEFs. These results support the hypothesis that activation of a compensating DNA damage response pathway in *Rad50$^{S/S}$* is the underlying basis for suppression of ATM deficiency in *Rad50$^{S/S}$ Atm$^{-/-}$* mice. This situation is reminiscent of the observation that a *S. cerevisiae rad50S* mutation is associated with partial suppression of the checkpoint defects in Mec1-deficient cells. These outcomes are dependent upon the Mec1 paralog, Tel1, and the Mre11 complex (Usui et al. 2001).

Rad50$^{S/S}$ did not mitigate phenotypic outcomes in *Mre11$^{ATLD1/ATLD1}$*. This may reflect that *Mre11$^{ATLD1/ATLD1}$* impairs the activity of both the alternative and the ATM-dependent pathway. Supporting this interpretation, *Mre11$^{ATLD1/ATLD1}$* is synthetically lethal with *Atm$^{-/-}$* (Table 1), as is *Nbs1$^{\Delta B/\Delta B}$* (Williams et al. 2002).

Since neither DNA-PKcs nor SMG1 have been implicated in the suppression of lymphomas, the alternative pathway is most likely to be ATR dependent. Consistent with this view, recent data suggest that Nbs1 influences the activity of ATR on certain targets (Stiff et al. 2004). However, the data in hand do not rigorously exclude a role for DNA-PKcs or SMG1 in the *Rad50$^{S/S}$*-dependent suppression of ATM deficiency. Irrespective of the kinase involved, the data clearly support the view that the influence of the Mre11 complex on the DNA damage response is not limited to ATM-dependent functions.

Finally, the suggestion that *Rad50$^{S/S}$* activates both ATM-dependent and ATM-independent responses may have therapeutic implications. On one hand, the fact that a pathway that mitigates ATM deficiency exists and can be activated may provide a basis for the development of treatments for ataxia-telangiectasia. On the other hand, the potent pro-apoptotic behavior of *Rad50^{S}* raises the possiblity that compounds mimicking this activity could be developed as anti-tumor agents that act with reduced mutagenic effects.

Materials and methods

Mice derivation and genotyping

Rad50$^{S/S}$, *Rad50$^{+/\Delta}$*, *Atm$^{-/-}$*, *Mre11$^{ATLD1/ATLD1}$*, *Nbs1$^{\Delta B/\Delta B}$*, *Chk2$^{-/-}$*, *Smc1$^{2SA/2SA}$* (= *Smc1$^{S957AS966A/S957AS966A}$*), and *Eμ-Bcl2* mice, survival, and genotyping have been described (Strasser et al. 1990; Barlow et al. 1996; Luo et al. 1999; Bender et al. 2002; Hirao et al. 2002; Williams et al. 2002; Theunissen et al. 2003; Kitagawa et al. 2004). All mice maintained on mixed 129/SvEv and C57BL6 background. *Rad50$^{S/S}$*, *Atm$^{-/-}$*, *Rad50$^{S/S}$ Atm$^{-/-}$*, and *Rad50$^{S/S}$ Atm$^{+/-}$* mice were derived at the University of Wisconsin Medical School and at Memorial Sloan-Kettering Cancer Center, and Figure 1B is a compilation of mice in both colonies. All other survival curves include mice born only at Memorial Sloan Kettering Cancer Center.

Cell derivation and culture

Murine embryonic fibroblasts (MEFs) and ear fibroblasts were generated and cultured as described (Bender et al. 2002). Immortalization was achieved by pX-8 transfection, an SV40 plasmid containing an inactivated origin of replication (Fromm and Berg 1982). For cumulative growth, the fold increase in cell number (R) was calculated from passage number 2 to passage number 6. Between each passage number, 100,000 cells were plated on six-well plates, and $R = X/100{,}000$ with X = cell number after 3 d. The cumulative cell number Y at each passage number (p) was obtained by solving $Y_{(p)} = Y_{(p-1)} \times R$ with $Y_{(2)} = 100{,}000$ and $p = 3, 4, 5$, and 6.

Survival analyses

Statistical significance determined by Wilcoxon Rank Sum Test or Fisher's exact test using Mstat software (Norman Drink-

Table 1. *Synthetic lethality of* Atm$^{-/-}$ Mre11$^{ATLD1/ATLD1}$

Genotype father	Genotype mother	Total no. of pups	Expected no. of double mutants[a]	Observed no. of double mutants	*P*-value[b]
Atm$^{+/-}$ Mre11$^{+/ATLD1}$	*Atm$^{+/-}$ Mre11$^{+/ATLD1}$*	245	4.8	0	7.8×10^{-3}
Atm$^{+/-}$ Mre1$^{ATLD1/ATLD1}$	*Atm$^{+/-}$ Mre11$^{+/ATLD1}$*	112	7.8	0	3.0×10^{-4}

[a]The number of expected double mutants is calculated based on a physical distance of 28 centimorgans (cM) between the *ATM* and *MRE11* loci. On the Mouse Genome Informatics Web site (http://www.informatics.jax.org), the *ATM* locus maps to 30 cM on chromosome 9 and *GPR83* (a marker 25,820 bp from the *MRE11* Ensembl Transcript Report [http://www.ensemble.org]) maps to 2 cM on chromosome 9.
[b]*P*-value based on binomial distribution.

water, McArdle Laboratory for Cancer Research). Kaplan Meier survival curves made with Prism 4 (GraphPad Software).

Hematopoietic cell preparation and analysis

Single-cell suspensions from the thymus and bone marrow prepared and analyzed as described (Bender et al. 2002). Briefly, the number of DN T cells was equal to the number of CD4 CD8 double-negative cells in the thymus, the number of macrophages was equal to the number of the B220-negative and CD43-positive bone marrow cells, and the number of pro-B cells was equal to the number of B220 CD43 double-positive bone marrow cells.

Cellular assays

Sensitivity to IR, intra-S-phase, and G2/M checkpoint functions assessed as described (Williams et al. 2002). Cells were irradiated with a Mark I 137Cs source at 222 cGy/min. G1/S checkpoint assays carried out as described (Xu et al. 1996). Chromosomal analyses were prepared as described previously (Bender et al. 2002) and carried out on blinded samples. Splenocytes were stimulated with lipopolysaccharide for 48 h prior to addition of colcemid for 3 h. Ear fibroblasts were incubated for 4 h with colcemid.

Immunohistochemistry

Four percent paraformaldehyde-fixed tissues were processed at the Research Animal Resource Center of the Cornell University Medical College. Paraffin-embedded 5–10-µm sections were stained with hematoxylin and eosin, and cleaved Caspase-3 (Cell Signalling; #9661) immunohistochemistry was performed at the Molecular Cytology Core Facility of Memorial Sloan-Kettering Cancer Center. Color images were captured using a Nikon digital camera and processed using Adobe Photoshop.

Immunoprecipitations and Western blotting

For 53BP1 IP, whole-cell extracts of primary ear fibroblasts were obtained in lysis buffer (300 mM NaCl, 20 mM Hepes at pH 7.9 and 0.5% NP-40 with protease and phosphatase inhibitors). One microgram of 53BP1-Ser25-P antibody (gift from P. Carpenter, Harvard Medical School, Boston, MA) was added to the extracts for 30 min, and proteins were immunoprecipitated for 1 h with protein A/G agarose. IPs were washed twice with wash buffer (150 mM NaCl, 20 mM Hepes at pH 7.9 and 0.5% NP-40 with protease and phosphatase inhibitors) and loaded on a gel. Lysates for Western blot were obtained in lysis buffer (200–400 mM NaCl, 50 mM Tris-HCl at pH 7.5, 1% NP-40 with protease and phosphatase inhibitors). To prepare extracts for γ-H2AX detection, the chromatin pellet from regular lysates was further incubated for 30 min in 0.1 M HCl, and the resulting supernatant was used for immunoblotting. Chk2 (Upstate Biotechnology; 05-649) antiserum used at 1:400 dilution in 2% BSA/PBS. 53BP1 (gift from P. Carpenter) and γ-H2AX (Cell Signaling) antisera used at a 1:500 dilution in 5% Milk/0.1% Tween/PBS (MTP). p53 (Novacastra; NCL-p53-CM5p), p53-Ser15-P (Cell Signaling; #9284), SMC1-Ser957-P (Cell Signaling; #4805), and ATM-Ser1981-P (Cell Signaling; #4526) antisera were used at 1:1000 dilution in MTP. Actin (Sigma; A4700), PCNA (Calbiochem; NA03), SMC1 (Novus Biologicals; ab9262), and ATM (MAT3; gift from Y. Shiloh, Sackler School of Medicine, Tel Aviv University, Tel Aviv, Israel) antisera were used at 1:2000 dilution in MTP. For ATM detection, IPs and lysates were loaded on 3%–8% Tris-Acetate gels (NuPAGE, Invitrogen).

Immunofluorescence assays

Immunofluorescence experiments were done as previously described (Maser et al. 1997). SQ/TQ antibody (Cell Signaling; #2851) was used at a 1:500 dilution in 1% BSA/PBS.

Acknowledgments

We are grateful to Fred Alt and David Ferguson for SKY analyses for $Atm^{-/-}$ and $Rad50^{S/S}$ $Atm^{-/-}$ splenocytes, and Tak Mak and Howard Petrie for mouse strains. We thank Doug Bishop and members of the Petrini laboratory for insights, and Andy Koff and Scott Keeney for critical reading of the manuscript. This work was supported by NIH grants GM56888, CA03632, and CA21765, and the Joel and Joan Smilow Initiative.

References

Abraham, R.T. 2004. PI 3-kinase related kinases: 'Big' players in stress-induced signaling pathways. *DNA Repair* **3:** 883–887.

Bakkenist, C.J. and Kastan, M.B. 2003. DNA damage activates ATM through intermolecular autophosphorylation and dimer dissociation. *Nature* **421:** 499–506.

Barlow, C., Hirotsune, S., Paylor, R., Liyanage, M., Eckhaus, M., Collins, F., Shiloh, Y., Crawley, J.N., Ried, T., Tagle, D., et al. 1996. Atm-deficient mice: A paradigm of ataxia telangiectasia. *Cell* **86:** 159–171.

Bassing, C.H., Suh, H., Ferguson, D.O., Chua, K.F., Manis, J., Eckersdorff, M., Gleason, M., Bronson, R., Lee, C., and Alt, F.W. 2003. Histone H2AX: A dosage-dependent suppressor of oncogenic translocations and tumors. *Cell* **114:** 359–370.

Bender, C.F., Sikes, M.L., Sullivan, R., Huye, L.E., Le Beau, M.M., Roth, D.B., Mirzoeva, O.K., Oltz, E.M., and Petrini, J.H. 2002. Cancer predisposition and hematopoietic failure in Rad50(S/S) mice. *Genes & Dev.* **16:** 2237–2251.

Bosma, G., Custer, R., and Bosma, M. 1983. A severe combined immunodeficiency mutation in mice. *Nature* **301:** 527–530.

Brumbaugh, K.M., Otterness, D.M., Geisen, C., Oliveira, V., Brognard, J., Li, X., Lejeune, F., Tibbetts, R.S., Maquat, L.E., and Abraham, R.T. 2004. The mRNA surveillance protein hSMG-1 functions in genotoxic stress response pathways in mammalian cells. *Mol. Cell* **14:** 585–598.

Burma, S., Chen, B.P., Murphy, M., Kurimasa, A., and Chen, D.J. 2001. ATM phosphorylates histone H2AX in response to DNA double-strand breaks. *J. Biol. Chem.* **276:** 42462–42467.

Carney, J.P., Maser, R.S., Olivares, H., Davis, E.M., Le Beau, M., Yates III, J.R., Hays, L., Morgan, W.F., and Petrini, J.H. 1998. The hMre11/hRad50 protein complex and Nijmegen breakage syndrome: Linkage of double-strand break repair to the cellular DNA damage response. *Cell* **93:** 477–486.

Carson, C.T., Schwartz, R.A., Stracker, T.H., Lilley, C.E., Lee, D.V., and Weitzman, M.D. 2003. The Mre11 complex is required for ATM activation and the G(2)/M checkpoint. *EMBO J.* **22:** 6610–6620.

Celeste, A., Difilippantonio, S., Difilippantonio, M.J., Fernandez-Capetillo, O., Pilch, D.R., Sedelnikova, O.A., Eckhaus, M., Ried, T., Bonner, W.M., and Nussenzweig, A. 2003. H2AX haploinsufficiency modifies genomic stability and tumor susceptibility. *Cell* **114:** 371–383.

Costanzo, V., Paull, T., Gottesman, M., and Gautier, J. 2004. Mre11 assembles linear DNA fragments into DNA damage signaling complexes. *PLoS Biol.* **2:** E110.

D'Amours, D. and Jackson, S.P. 2002. The Mre11 complex: At the crossroads of DNA repair and checkpoint signalling. *Nat.*

Rev. Mol. Cell. Biol. **3:** 317–327.
de Jager, M. and Kanaar, R. 2002. Genome instability and Rad50(S): Subtle yet severe. *Genes & Dev.* **16:** 2173–2178.
Difilippantonio, M.J., Zhu, J., Chen, H.T., Meffre, E., Nussenzweig, M.C., Max, E.E., Ried, T., and Nussenzweig, A. 2000. DNA repair protein Ku80 suppresses chromosomal aberrations and malignant transformation. *Nature* **404:** 510–514.
Difilippantonio, S., Celeste, A., Fernandez-Capetillo, O., Chen, H.T., Reina San Martin, B., Van Laethem, F., Yang, Y.P., Petukhova, G.V., Eckhaus, M., Feigenbaum, L., et al. 2005. Role of Nbs1 in the activation of the Atm kinase revealed in humanized mouse models. *Nat. Cell. Biol.* **7:** 675–685.
Essers, J., Hendriks, R.W., Swagemakers, S.M., Troelstra, C., de Wit, J., Bootsma, D., Hoeijmakers, J.H., and Kanaar, R. 1997. Disruption of mouse RAD54 reduces ionizing radiation resistance and homologous recombination. *Cell* **89:** 195–204.
Falck, J., Coates, J., and Jackson, S.P. 2005. Conserved modes of recruitment of ATM, ATR and DNA-PKcs to sites of DNA damage. *Nature* **434:** 605–611.
Fromm, M. and Berg, P. 1982. Deletion mapping of DNA regions required for SV40 early region promoter function in vivo. *J. Mol. Appl. Genet.* **1:** 457–481.
Gatei, M., Young, D., Cerosaletti, K.M., Desai-Mehta, A., Spring, K., Kozlov, S., Lavin, M.F., Gatti, R.A., Concannon, P., and Khanna, K. 2000. ATM-dependent phosphorylation of nibrin in response to radiation exposure. *Nat. Genet.* **25:** 115–119.
Hirao, A., Cheung, A., Duncan, G., Girard, P.M., Elia, A.J., Wakeham, A., Okada, H., Sarkissian, T., Wong, J.A., Sakai, T., et al. 2002. Chk2 is a tumor suppressor that regulates apoptosis in both an ataxia telangiectasia mutated (ATM)-dependent and an ATM-independent manner. *Mol. Cell. Biol.* **22:** 6521–6532.
Horejsi, Z., Falck, J., Bakkenist, C.J., Kastan, M.B., Lukas, J., and Bartek, J. 2004. Distinct functional domains of Nbs1 modulate the timing and magnitude of ATM activation after low doses of ionizing radiation. *Oncogene* **23:** 3122–3127.
Kang, J., Bronson, R., and Xu, Y. 2002. Targeted disruption of NBS1 reveals its roles in mouse development and DNA repair. *EMBO J.* **21:** 1447–1455.
Keeney, S. and Kleckner, N. 1995. Covalent protein–DNA complexes at the 5′ strand termini of meiosis- specific double-strand breaks in yeast. *Proc. Natl. Acad. Sci.* **92:** 11274–11278.
Kim, S.T., Lim, D.S., Canman, C.E., and Kastan, M.B. 1999. Substrate specificities and identification of putative substrates of ATM kinase family members. *J. Biol. Chem.* **274:** 37538–37543.
Kim, S.-T., Xu, B., and Kastan, M.B. 2002. Involvement of the cohesin protein Smc1, in Atm-dependent and independent responses to DNA damage. *Genes & Dev.* **16:** 560–570.
Kitagawa, R., Bakkenist, C.J., McKinnon, P.J., and Kastan, M.B. 2004. Phosphorylation of SMC1 is a critical downstream event in the ATM–NBS1–BRCA1 pathway. *Genes & Dev.* **18:** 1423–1438.
Lee, J.H. and Paull, T.T. 2005. ATM activation by DNA double-strand breaks through the Mre11–Rad50–Nbs1 complex. *Science* **308:** 551–554.
Lim, D.S., Kim, S.T., Xu, B., Maser, R.S., Lin, J., Petrini, J.H., and Kastan, M.B. 2000. ATM phosphorylates p95/nbs1 in an S-phase checkpoint pathway. *Nature* **404:** 613–617.
Ludwig, T., Fisher, P., Ganesan, S., and Efstratiadis, A. 2001. Tumorigenesis in mice carrying a truncating Brca1 mutation. *Genes & Dev.* **15:** 1188–1193.
Luo, G., Yao, M.S., Bender, C.F., Mills, M., Bladl, A.R., Bradley, A., and Petrini, J.H. 1999. Disruption of mRad50 causes embryonic stem cell lethality, abnormal embryonic development, and sensitivity to ionizing radiation. *Proc. Natl. Acad. Sci.* **96:** 7376–7381.
Maser, R.S., Monsen, K.J., Nelms, B.E., and Petrini, J.H. 1997. hMre11 and hRad50 nuclear foci are induced during the normal cellular response to DNA double-strand breaks. *Mol. Cell. Biol.* **17:** 6087–6096.
McPherson, J.P., Lemmers, B., Chahwan, R., Pamidi, A., Migon, E., Matysiak-Zablocki, E., Moynahan, M.E., Essers, J., Hanada, K., Poonepalli, A., et al. 2004. Involvement of mammalian Mus81 in genome integrity and tumor suppression. *Science* **304:** 1822–1826.
Mochan, T.A., Venere, M., DiTullio Jr., R.A., and Halazonetis, T.D. 2003. 53BP1 and NFBD1/MDC1-Nbs1 function in parallel interacting pathways activating ataxia-telangiectasia mutated (ATM) in response to DNA damage. *Cancer Res.* **63:** 8586–8591.
Nairz, K. and Klein, F. 1997. mre11S—A yeast mutation that blocks double-strand-break processing and permits nonhomologous synapsis in meiosis. *Genes & Dev.* **11:** 2272–2290.
Neale, M.J., Pan, J., and Keeney, S. 2005. Endonucleolytic processing of covalent protein-linked DNA double-strand breaks. *Nature* **436:** 1053–1057.
Petrini, J.H. 2000. The Mre11 complex and ATM: Collaborating to navigate S phase. *Curr. Opin. Cell. Biol.* **12:** 293–296.
Petrini, J.H. and Stracker, T.H. 2003. The cellular response to DNA double-strand breaks: Defining the sensors and mediators. *Trends Cell. Biol.* **13:** 458–462.
Stewart, G.S., Maser, R.S., Stankovic, T., Bressan, D.A., Kaplan, M.I., Jaspers, N.G., Raams, A., Byrd, P.J., Petrini, J.H., and Taylor, A.M. 1999. The DNA double-strand break repair gene hMRE11 is mutated in individuals with an ataxia-telangiectasia-like disorder. *Cell* **99:** 577–587.
Stiff, T., Reis, C., Alderton, G.K., Woodbine, L., O'Driscoll, M., and Jeggo, P.A. 2004. Nbs1 is required for ATR-dependent phosphorylation events. *EMBO J* **24:** 199–208.
Stohr, B.A. and Kreuzer, K.N. 2001. Repair of topoisomerase-mediated DNA damage in bacteriophage t4. *Genetics* **158:** 19–28.
Stojic, L., Mojas, N., Cejka, P., Di Pietro, M., Ferrari, S., Marra, G., and Jiricny, J. 2004. Mismatch repair-dependent G2 checkpoint induced by low doses of SN1 type methylating agents requires the ATR kinase. *Genes & Dev.* **18:** 1331–1344.
Stracker, T.H., Carson, C.T., and Weitzman, M.D. 2002. Adenovirus oncoproteins inactivate the Mre11–Rad50–NBS1 DNA repair complex. *Nature* **418:** 348–352.
Stracker, T.H., Theunissen, J.W., Morales, M., and Petrini, J.H. 2004. The Mre11 complex and the metabolism of chromosome breaks: The importance of communicating and holding things together. *DNA Repair* **3:** 845–854.
Strasser, A., Harris, A.W., Vaux, D.L., Webb, E., Bath, M.L., Adams, J.M., and Cory, S. 1990. Abnormalities of the immune system induced by dysregulated bcl-2 expression in transgenic mice. *Curr. Top. Microbiol. Immunol.* **166:** 175–181.
Strasser, A., Harris, A.W., and Cory, S. 1991a. bcl-2 transgene inhibits T cell death and perturbs thymic self-censorship. *Cell* **67:** 889–899.
Strasser, A., Whittingham, S., Vaux, D.L., Bath, M.L., Adams, J.M., Cory, S., and Harris, A.W. 1991b. Enforced BCL2 expression in B-lymphoid cells prolongs antibody responses and elicits autoimmune disease. *Proc. Natl. Acad. Sci.* **88:** 8661–8665.
Theunissen, J.W., Kaplan, M.I., Hunt, P.A., Williams, B.R., Ferguson, D.O., Alt, F.W., and Petrini, J.H. 2003. Checkpoint

failure and chromosomal instability without lymphomagenesis in Mre11(ATLD1/ATLD1) mice. *Mol. Cell* **12:** 1511–1523.

Tsubouchi, H. and Ogawa, H. 1998. A novel mre11 mutation impairs processing of double-strand breaks of DNA during both mitosis and meiosis. *Mol. Cell. Biol.* **18:** 260–268.

Usui, T., Ogawa, H., and Petrini, J.H. 2001. A DNA damage response pathway controlled by Tel1 and the Mre11 complex. *Mol. Cell* **7:** 1255–1266.

Uziel, T., Lerenthal, Y., Moyal, L., Andegeko, Y., Mittelman, L., and Shiloh, Y. 2003. Requirement of the MRN complex for ATM activation by DNA damage. *EMBO J.* **22:** 5612–5621.

Ward, I.M. and Chen, J. 2001. Histone H2AX is phosphorylated in an ATR-dependent manner in response to replicational stress. *J. Biol. Chem.* **276:** 47759–47762.

Williams, B.R., Mirzoeva, O.K., Morgan, W.F., Lin, J., Dunnick, W., and Petrini, J.H. 2002. A murine model of nijmegen breakage syndrome. *Curr. Biol.* **12:** 648–653.

Wu, X., Ranganathan, V., Weisman, D.S., Heine, W.F., Ciccone, D.N., O'Neill, T.B., Crick, K.E., Pierce, K.A., Lane, W.S., Rathbun, G., et al. 2000. ATM phosphorylation of Nijmegen breakage syndrome protein is required in a DNA damage response. *Nature* ***405:*** **477–482.**

Xu, Y. and Baltimore, D. 1996. Dual roles of ATM in the cellular response to radiation and in cell growth control. *Genes & Dev.* **10:** 2401–2410.

Xu, Y., Ashley, T., Brainerd, E.E., Bronson, R.T., Meyn, M.S., and Baltimore, D. 1996. Targeted disruption of ATM leads to growth retardation, chromosomal fragmentation during meiosis, immune defects, and thymic lymphoma. *Genes & Dev.* **10:** 2411–2422.

Yazdi, P.T., Wang, Y., Zhao, S., Patel, N., Lee, E.Y., and Qin, J. 2002. SMC1 is a downstream effector in the ATM/NBS1 branch of the human S-phase checkpoint. *Genes & Dev.* **16:** 571–582.

You, Z., Chahwan, C., Bailis, J., Hunter, T., and Russell, P. 2005. ATM activation and its recruitment to damaged DNA require binding to the C terminus of Nbs1. *Mol. Cell. Biol.* **25:** 5363–5379.

Zhao, S., Weng, Y.C., Yuan, S.S., Lin, Y.T., Hsu, H.C., Lin, S.C., Gerbino, E., Song, M.H., Zdzienicka, M.Z., Gatti, R.A., et al. 2000. Functional link between ataxia-telangiectasia and Nijmegen breakage syndrome gene products. *Nature* **405:** 473–477.